STABILITY, ELECTRONIC STRUCTURE, AND PHASE DIAGRAMS OF NOVEL INTER-SEMICONDUCTOR COMPOUNDS

L. G. Ferreira,
S.-H. Wei, and
Alex Zunger

SOLAR ENERGY RESEARCH INSTITUTE
GOLDEN, COLORADO 80401

Summary

High-technology electronic devices are based on highly specialized core materials that make their operation possible: semiconductors. Unfortunately, the range of material properties that make high-technology devices work is extremely narrow, since the sheer number of useful semiconductors is small. Hence, a major challenge has been to predict and develop new, potentially useful semiconductors. We describe here how the use of state-of-the-art techniques in both quantum and statistical mechanics can lead to predictions of new, stable, and ordered semiconductor alloys. A number of laboratories have already grown experimentally these new materials; efforts to characterize their useful material properties are ongoing in the United States, Japan, and Europe. This work describes the theoretical methodologies of our approach, and shows how supercomputers make possible the quantum-mechanical architectural analysis of new materials.

Introduction

Simple semiconductors such as Si, Ge, GaP, GaAs, InP, and AℓAs have traditionally been used as core materials for a wide range of electronic and optoelectronic devices, including integrated circuits, lasers, light-emitting diodes, solar cells, and various light-detectors. Since the existing number of such simple semiconductors is small [O(10)], they provide but a limited range of material properties (bandgaps, carrier mobilities, lattice parameters). It has hence been a common practice to form solid solutions (of composition x) A_xB_{1-x} of the parent compounds A and B, attempting thereby to obtain technologically useful material properties that are intermediate between those of pure A and pure B. Unlike the parent crystalline semiconductors A and B, however, the alloys A_xB_{1-x} are disordered, and hence generally have lesser electron mobility, and are structurally unstable toward low-temperature disproportionation into their binary constituents (their mixing enthalpy ΔH is positive, so their free energy $\Delta H - TS$ is negative only at sufficiently high temperature T, where the $-TS$ entropy term overwhelms ΔH). Until recently (Panish and Ilegems, 1972; Stringfellow, 1973), it was believed that all such isovalent semiconductor alloys between A and B (where A and B are either IV-IV, III-V, or II-VI semiconductors) exist either as disproportionation products $A + B$, or as disordered solid solutions A_xB_{1-x}. More recently we have predicted theoretically that hitherto unknown, long-range, *ordered* stoichiometric inter-semiconductor compounds A_nB_m can be thermodynamically stabler than the disordered alloy below some growth temperature T_c (Srivastara, Martins, and Zunger, 1985; Zunger, 1986; Martins and Zunger, 1986). Such ordered compounds form a novel class of semiconductors in that their crystal structures are unprecedented in conventional semiconductor physics (they can appear in tetragonal CuAuI-like, rhombohedral CuPt-like, or chalcopyrite-like modifications, see Fig. 1); their band structures (hence, bandgaps, effective masses, etc.) differ either from the average of the constituents or from those of the disordered alloy; and many of them are thermodynamically stabler (i.e., have lower ΔH) than the disordered alloy of the same composition; some are even

The International Journal of Supercomputer Applications, Volume 5, No. 1, Spring 1991, pp. 34–56.

Ordering Vector	**(0,0,0)**	**(0,0,1)**			**(2,0,1)**		**(1,1,1)**
Name	**Zincblende (Sphalerite)**	**Layered tetragonal**	**"Luzonite"**	**2 layer superlattice**	**Chalcopyrite**	**Famatinite**	**Layered Trigonal**
Formula:	n = 0,4:AC	n = 2;ABC_2	n = 1,3; A_3BC_4	n = 2;ABC_2	n = 2;ABC_2	n = 1,3; A_3BC_4	n = 2;ABC_2
	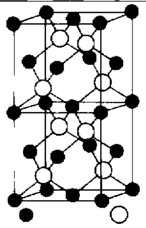 ● Zn ○ S	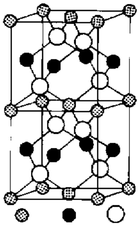 ▨ In ● Ga ○ As	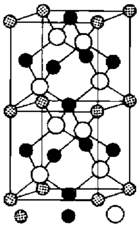 ▨ As ● Cu ○ S	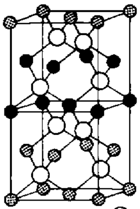 ▨ Al ● Ga ○ As	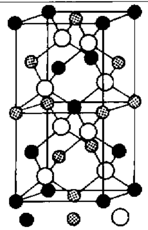 ● Cu ▨ Fe ○ S	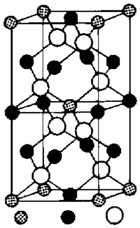 ▨ Sb ● Cu ○ S	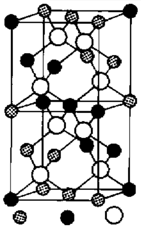 ▨ A ● B ○ C
Example: (ternary)	**ZnS-type**	**$InGaAs_2$-type (CA)**	**Cu_3AsS_4-type (L1 Or L3)**	**$(AlAs)_2(GaAs)_2$ (Z2)**	**$CuFeS_2$-type (CH)**	**Cu_3SbS_4-type (F1 or F3)**	**$CrCuS_2$-type (CP)**
Bravais Lattice:	Face centered cubic	Simple tetragonal	Simple cubic	Simple tetragonal	Body centered tetragonal	Body centered tetragonal	Rhombohedral
Space Group							
Int. Tables:	$F\bar{4}3m$	$P\bar{4}m2$	$P\bar{4}3m$	$P\bar{4}2m$	$I\bar{4}2d$	$I\bar{4}2m$	$R3m$
Schoenflies:	T_d^2	D_{2d}^5	T_d^1	D_{2d}^5	D_{2d}^{12}	D_{2d}^{11}	C_{3v}^5

Fig. 1 Structural description of the new, inter-semiconductor phases

stabler than the phase-separated systems (Dandrea et al., 1990).

Since our original prediction, more than 20 observations of such long-range, ordered, inter-semiconductor compounds have been made (see Zunger and Wood, 1989, and compilation of references therein). It now appears that this phenomenon of long-range, ordered, inter-semiconductor phases is likely to be the rule rather than the exception in semiconductor physics.

It is obvious that direct calculations of the internal energies of such systems will not suffice to model their properties and stabilities. First, these are often stable only at finite temperatures, so usual quantum-mechanical calculations (appropriate to $T = 0$) do not suffice and a full thermodynamic theory is required. Second, even on a *fixed* lattice with N points, there are 2^N arrangements ("configurations") of A and B atoms. Since this can be a truly astronomical number, it is impractical to calculate directly the energies of such a large number of configurations in an effort to delineate the stability of ordered and disordered (or phase-separated) configurations. Hence we set out to formulate a general theory of thermodynamic stability of $A_{1-x}B_x$ alloys using a combination of quantum and statistical mechanics. The objective was to advance a detailed theory of electronic properties and phase diagrams of inter-semiconductor phases.

We first describe the essential physics, the mathematical approach, and the computer algorithm used for identifying stable structures.

Statement of the Physical Problem

The energy of any configuration σ (any arrangement of atoms A and B on a lattice with N sites) can be written as an Ising-like expression

$$E(\sigma) = \sum_f J_f \Pi_f(\sigma), \qquad (1)$$

where f is an elementary "figure" with k_f vertices, (i.e., a certain selection of k_f sites out of the total N lattice sites) and $\Pi_f(\sigma)$ is the product of spins at the vertices of $f(\hat{S} = +1$ if the site has an atom B, and -1 if A):

$$\Pi_f(\sigma) = \hat{S}_{1_f}\hat{S}_{2_f} \ldots \hat{S}_{k_f}. \qquad (2)$$

Equation (1) can be written for any property that is defined for all 2^N possible configurations σ, for example, energy, molar volume, and bulk modulus. This assertion is based on the orthogonality properties of the products $\Pi_f(\sigma)$ (Sanchez, Ducastelle, and Gratias, 1984):

$$\sum_\sigma \Pi_f(\sigma)\Pi_g(\sigma) = 2^N \delta_{f,g}, \qquad (3)$$

and

$$\sum_f \Pi_f(\sigma)\Pi_f(\sigma') = 2^N \delta_{\sigma,\sigma'}. \qquad (4)$$

Since the energy $E(\sigma)$ is defined for any configuration σ, we can define the interaction parameters J_f by using Eq. (1) and Eq. (3), which give

$$J_f = 2^{-N} \sum_\sigma E(\sigma)\Pi_f(\sigma). \qquad (5)$$

Equations (1) and (5) serve well to define the physical content of a microscopic alloy theory. What is needed is the following:

1. A microscopic theory of the basic cluster interactions $\{J_f\}$. In general, $\{J_f\}$ depend on the chemical properties of A and B, their relative sizes, the alloy composition, and the Bravais lattice (e.g., fcc, bcc). We will hence formulate a self-consistent electronic structure theory whereby $\{J_f\}$ are computed (quantum mechanically) from band theory.
2. An examination of the convergence of Eq. (1) with respect to the range of interactions. This was reported by Ferreira, Wei, and Zunger (1989) and will be only briefly noted here.
3. Having established an ab initio and practically complete set of interactions $\{J_f\}$, one needs next to search all 2^N configurations to establish the compounds that form a $T = 0$ ground state.
4. Finally, a finite-temperature theory is constructed whereby one finds the temperature and composition ranges where certain phases are stable (a phase diagram). This is done through the cluster variation method (CVM) and Monte Carlo simulations.

Since steps 1, 2, and 4 were described recently in some detail, we will give only a brief description and references to these items, and focus in more detail on step 3, that is, the description of a new computer algorithm for finding ground states.

Approach

THE CLUSTER EXPANSION

Expansions such as Eq. (1) are useful only when they converge reasonably rapidly in the sense that the interactions are nonnegligible only for atoms that are not far apart. To increase the speed of convergence, it is possible to make the interactions volume-dependent (Connolly and Williams, 1983); hence Eq. (1) reads

$$E(\sigma,V) = \sum_f J_f(V)\Pi_f(\sigma), \qquad (6)$$

in which case the equilibrium volume is determined by

$$\frac{dE(\sigma,V)}{dV} = \sum_f \frac{dJ_f(V)}{dV}\Pi_f(\sigma) = 0, \qquad (7)$$

or, to separate an elastic piece $G(x)$ from $E(\sigma)$ (Ferreira, Mbaye, and Zunger, 1988)

$$E(\sigma) = G(x) + \sum_f V_f \Pi_f(\sigma). \qquad (8)$$

The sum in Eq. (1) can be reduced by symmetry. Letting $\hat{R}$ be an operation of the space group of the lattice (e.g., O_h^5 of the fcc lattice), we have

$$E(\hat{R}\sigma) = E(\sigma); \qquad (9)$$

that is, if we operate on the configuration σ, we obtain the configuration $\hat{R}\sigma$ with the same energy. Furthermore,

$$\Pi_{\hat{R}f}(\hat{R}\sigma) = \Pi_f(\sigma); \qquad (10)$$

that is, operating on the figure and on the configuration leads to the same product of spins. Then, from Eq. (5) we obtain

$$J_{\hat{R}f} = J_f,$$

implying that all figures related by symmetry have equal interaction energies. It is hence convenient to define the "lattice average product" (denoted by a bar):

$$\overline{\Pi}_F(\sigma) = \frac{1}{Ng_0}\sum_{\hat{R}} \Pi_{\hat{R}F}(\sigma), \qquad (11)$$

where Ng_0 is the number of operations $\hat{R}$ of the space group ($g_0 = 48$ for fcc). Equation (1) then reads

$$E(\sigma) = N\sum_F D_F J_F \overline{\Pi}_F(\sigma), \qquad (12)$$

where the sum is over the prototype figures F which are not related by symmetry to any other figure in the sum, and ND_F is the number of figures f related by symmetry to the prototype figure F. Figure 2 shows some main prototype figures for fcc and bcc lattices, respectively.

DETERMINING THE INTERACTION ENERGIES J_f

In many applications of the Ising model to alloys, the interaction energies $\{J_F\}$ of Eq. (12) were taken as ad hoc parameters (Kikuchi et al., 1980). Since we wish to understand the way in which the microscopic electronic interactions drive the stability of particular (ordered or

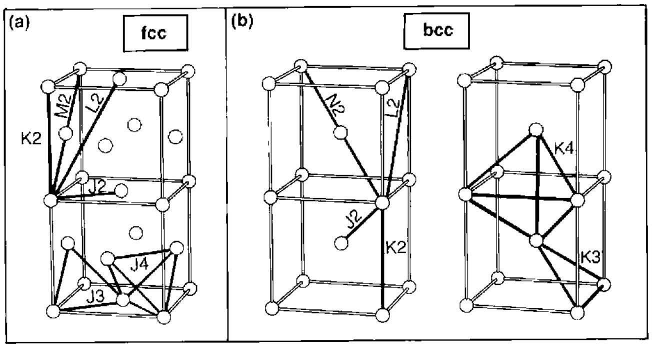

Fig. 2 Description of the basic figures used in the cluster expansion for (a) fcc and (b) bcc systems J2, K2, L2, M2, and N2 are pair interactions between first, second, third, fourth, and fifth neighbors, respectively, while J3 and K3 are three-body terms and J4 and K4 are four-body terms.

disordered) configurations, we next develop an electronic (quantum mechanical) theory for evaluating the interactions $\{J_F\}$.

> ***"In many applications of the Ising model to alloys, the interaction energies were taken as ad hoc parameters. Since we wish to understand the way in which the microscopic electronic interactions drive the stability of particular configurations, we next develop an electronic theory for evaluating the interactions."***

To the extent that a finite and "small" set of functions $\{J_F(V)\}$ can capture, through Eq. (12), the essential energetics of arbitrary configurations σ on a given substitutional lattice, we can determine $\{J_F(V)\}$ from the total energy of a corresponding set of simple periodic structures (Connolly and Williams, 1983; Srivastara, Martins, and Zunger, 1985; Ferreira, Wei, and Zunger, 1989). Specializing Eq. (12) to such ordered structures $\{s\}$, we have

$$\Delta E(s,V) = N \sum_F J_F(V) D_F \overline{\Pi}_F(s). \tag{13}$$

The left side of Eq. (13) is defined as the *excess* energy of s with respect to the same amount of pure constituents:

$$\Delta E(s,V) = E(A_nB_m,V) - \frac{n}{n+m} E(A_nA_m,V_A) - \frac{m}{n+m} E(B_nB_m,V_B). \tag{14}$$

Here, A_nA_m or B_nB_m denote the pure A and B solids, respectively. Note, therefore, that the scale of $\Delta E(s,V)$ is not that of the total energy of a given structure ($\sim 10^6$ eV for GaAs), or that of the cohesive energy ($\sim$5–7 eV for binary semiconductors), but rather the *relative* energy of A_nB_m with respect to its constituents ($\sim 10^{-2}$ eV). The large constant terms appearing in $E(s)$ (e.g., the sum of atomic energies) are cancelled in the construct of Eq. (14). We calculate $\Delta E(s,V)$ in the local density formalism (LDF) (Hohenberg and Kohn, 1964) as implemented by the general potential, linear augmented plane wave (LAPW) method (Wei and Krakauer, 1985) or by the pseudopotential plane wave method (Ihm, Zunger, and Cohen, 1979). The total LDF energy includes kinetic energy, interelectronic coulomb, exchange, and correlation terms, as well as the ion-ion and electron-ion interactions:

$$E(s,V) = \sum_i^{\epsilon_F} N_i \epsilon_i - \frac{1}{2}\int \rho(\mathbf{r})\chi(\mathbf{r})d\mathbf{r} - \frac{1}{2}\sum_\alpha Z_\alpha V_1(\boldsymbol{R}_\alpha), \tag{15a}$$

where

$$\chi(\mathbf{r}) = V_c(\mathbf{r}) + 2\{V_{xc}(\mathbf{r}) - \epsilon_{xc}(\mathbf{r})\}. \qquad (15b)$$

Here, N_i is the occupation number of level i below the Fermi energy ϵ_F; $\rho(r)$ is the electronic charge density obtained from the self-consistent single-particle wave functions; Z_α is the atomic number of atom α at $\boldsymbol{R}_\alpha$; $V_1(\boldsymbol{R}_\alpha)$ is the coulomb potential at $\boldsymbol{R}_\alpha$ due to all electrons and nuclei except the charge Z_α at $\boldsymbol{R}_\alpha$; V_c and V_{xc} are, respectively, the coulomb and electronic exchange-correlation potentials; and ϵ_{xc} is the exchange-correlation energy density. Solution of Eq. (15) requires first the solution of the Schrödinger equation, including (three-dimensional) coulomb, exchange, and correlation. This is the single most expensive step in the calculation. The charge density is determined self-consistently and variationally from the semirelativistic (i.e., retaining all relativistic terms but spin-orbit interactions) local density Hamiltonian. For each unit cell volume V, we minimize the total energy with respect to the cell-internal atomic coordinates, thereby obtaining relaxed energies. To ensure effective numerical cancellation of systematic errors in Eq. (14), we use for A_nB_m, A_nA_m, and B_nB_m precisely equivalent basis sets and integration methods, and sample the Brillouin zone by sets of wave-vectors $\mathbf{k}$ which are geometrically equivalent in A_nB_m, A_nA_m, and B_nB_m. We use for the zincblende structure the two special $\mathbf{k}$ points (Chadi and Cohen, 1973) and equivalent $\mathbf{k}$ points are used for all other structures. Convergence tests with respect to $\mathbf{k}$ point sampling show that the error in ΔE is less than 5 meV per four atoms.

> ***"The charge density is determined self-consistently and variationally from the semirelativistic local density Hamiltonian. For each unit cell volume, we minimize the total energy with respect to the cell-internal atomic coordinates, thereby obtaining relaxed energies."***

COMPUTATIONAL DIFFICULTIES IN THE QUANTUM MECHANICAL STEP

The excess total energy of structure s, Eq. (14), is of the order of $\sim 10^{-2}$ eV per atom; *differences* of excess energies between different structures are of the same order or smaller. Yet, the directly calculated total electron plus ion energy, E in Eq. (14), is of the order 10^5 to 10^7 eV per atom. Hence, extremely converged and precise calculations are needed. This energy is obtained by solving a Schrödinger equation with basis sets of the order of $N_b = 10^3$ basis functions. Storage of the relevant Hamiltonian matrices requires 1 to 1.5 million words and their diagonalization times scales as N_b^3 (however, our iterative diagonalization algorithm described by Wood and Zunger [1985] scales only as $\approx N_b^2$). For each structure we have to iterate the Schrödinger equation to self-consistency ($N_I = 5-7$ iterations per geometry). This is done using an efficient Jacobian update algorithm (Bendt and Zunger, 1982). At each iteration we have to sample the charge density at $N_k \sim 10$ points in the Brillouin zone. Each sampling requires diagonalization of the $N_b \times N_b$ Hamiltonian. The energy has to be optimized then with respect to atomic relaxations, requiring $N_R \sim 5$ geometry attempts per compound. This is done using the quantum mechanical force algorithm (Ihm, Zunger, and Cohen, 1979). The number of structures treated is $N_s \sim 10$. The work involved scales as $N_s \times N_I \times N_k \times N_R = 10 \times 6 \times 10 \times 5 = 3{,}000$ diagonalizations of the $N_b \times N_b$ Hamiltonian, where the precision required (see order of magnitude of the energy differences above) is very stringent. Calculations for a single compound take 20 to 50 CRAY Y-MP hours (depending if it has localized d electrons or not).

CONVERGENCE OF THE CLUSTER EXPANSION

As Connolly and Williams (1983) have shown, for a nonsingular $\det|\overline{\Pi}_f(s)| \neq 0$ in Eq. (13), knowledge of N_s equations of state $\Delta E(s,V)$ provides the N_s interaction energy functions

$$J_F(V) = \frac{1}{ND_F}\sum_{s}^{N_s}[\overline{\Pi}_F(s)]^{-1}\Delta E(s,V). \qquad (16)$$

This permits expression of the excess energy of general configurations σ of Eq. (6) as a linear combination of equations of state of periodic structures

$$\Delta E(\sigma,V) = \sum_{s}^{N_s}\xi_s(\sigma)\Delta E(s,V), \qquad (17)$$

where the weights are

$$\xi_s(\sigma) = \sum_{F}[\overline{\Pi}_F(s)]^{-1}\overline{\Pi}_F(\sigma). \qquad (18)$$

The key problem is to find a set of structures $\{s\}$ and figures $\{F\}$ that effect rapid convergence of Eq. (13) and Eq. (16). The procedure used is as follows: we select a set of N_s periodic structures $\{s\}$ (Fig. 1), compute the excess total energies $\{\Delta E(s,V)\}$ from electronic structure theory in Eq. (14) and Eq. (15), and obtain from Eq. (16) the N_s interaction energy functions $\{J_f(V)\}$ for the figures f depicted in Figure 2. This set is then used in the series expansion of Eq. (13) to predict the total energies $\{\Delta E(s',V)\}$ for another set $\{s'\} \neq \{s\}$ of periodic structures. This prediction is compared with the directly calculated values of $\Delta E(s',V)$ from electronic structure theory. The difference between the energies $\{\Delta E(s',V)\}$ obtained from the series expansion prediction and the "exact" (e.g., LAPW) excess energies is then minimized by varying the number and types of figures $\{F\}$ used in Eq. (12), establishing the minimum sizes of figures required to produce a given maximum error we are prepared to tolerate. Our study of isovalent zincblende semiconductor alloys (Ferreira, Wei, and Zunger, 1989; Wei, Ferreira, and Zunger, 1990) showed that to achieve a relative error of only a few percent in ΔE requires retention in Eq. (12) of up to *fourth fcc neighbors and up to four-body interactions.* These include eight $J_{k,m}$ terms (Fig. 2): (1) a normalization term $J_{0,1}$; (2) a sites-only term $J_{1,1}$; (3) four pair interaction terms, $J_{2,1}$, $J_{2,2}$, $J_{2,3}$, and $J_{2,4}$, between first, second, third, and fourth fcc neighbors, respectively (abbreviated in what follows and in Figure 2 as J_2, K_2, L_2, and M_2, respectively); and (4) a three-body $J_{3,1}$ ($\equiv J3$) and a four-body $J_{4,1}$ ($\equiv J4$) nearest-neighbor term. Our previous study (Ferreira, Wei, and Zunger, 1989) has also established an optimal set of structures $\{s\}$ consistent with the above requirements. Figure 1 depicts these structures, gives their space groups, ordering vectors, Bravais lattices, and the notation used to designate them.

THE ϵ-G REPRESENTATION

In what follows, it would be convenient to use the volume-dependent representation of Eq. (12) along with an equivalent ("ϵ-G") representation in which $\{J_F(V)\}$ are transformed into a volume-independent set $\{v_F\}$. This is done by separating Eq. (12) into "chemical" (ϵ) and "elastic" (G) pieces. For a general configuration σ at the equilibrium volume $V_{eq} = V(x)$, this separation reads

$$\Delta U(\sigma,V) = \epsilon(\sigma) + G(x). \qquad (19)$$

This is done (Ferreira, Mbaye, and Zunger, 1987, 1988; Ferreira, Wei, and Zunger, 1989) by requiring that

$\Delta U(s,V)$ have the same value for the first three volume derivatives as $\Delta E(s,V)$ of Eq. (13). In these references we have shown that this yields

$$G(x) = (1 - x)\int_0^x yZ(y)dy + x\int_X^1 (1 - y)Z(y)dy, \qquad (20)$$

where

$$Z(x) = \sum_n \left[Z_n + (x - X_n)\left(Z'_n - \sum_{j\neq n}\frac{2Z_n}{X_n - X_j}\right)\right] \qquad (21a)$$
$$\prod_{j\neq n}\frac{(x - x_j)^2}{(x_n - x_j)^2},$$

and

$$Z_n = Z(X_n) = \frac{B_n}{V_n}\left(\frac{dV}{dx}\right)^2. \qquad (21b)$$

Here B and V are the bulk modulus and molar volume, respectively. With $Z(x)$ defined as above, $\Delta U(s,V)$ of Eq. (19) has all the required properties of $\Delta E(s,V)$. Because the function $\Delta U(s,V)$ has the virtue that its volume-dependent term is linear in composition, the configurational energy can be separated as

$$\Delta U(\sigma,V) = G(x) + \sum_F D_F v_F \overline{\Pi}_F(\sigma) \qquad (22)$$

where v_F are *volume-independent* interactions energies given, in analogy with Eq. (16), by

$$v_F = \frac{1}{ND_F}\sum_s [\overline{\Pi}_F(s)]^{-1}\epsilon(s). \qquad (23)$$

Equations (22) and (23) are obtained from first-principles electronic structure calculations, much like Eq. (12), but are more convenient for ground-state searches.

SEARCHING THE GROUND STATE

At this point, we have a formulation of the configurational energy $E(\sigma)$ as a series expansion either in volume-dependent energies, Eq. (12), or in volume-independent energies plus a "source" term, Eq. (22). In either case, the basic interaction energies are described through a quantum-mechanical formulation of the total Born-Oppenheimer energy, Eq. (15), that is, by Eq. (16) for $\{J_F(V)\}$, or by Eq. (23) for $\{v_F\}$. In both cases, the

> ***"Our study suggests that the thermodynamic properties of bulk isovalent zincblende semiconductor alloys can be quantitatively understood in terms of a general Ising model with up to fourth-neighbor interactions. The global trends can be understood by separating the excess enthalpy into a volume-dependent term and a sum over volume-independent configurational energies."***

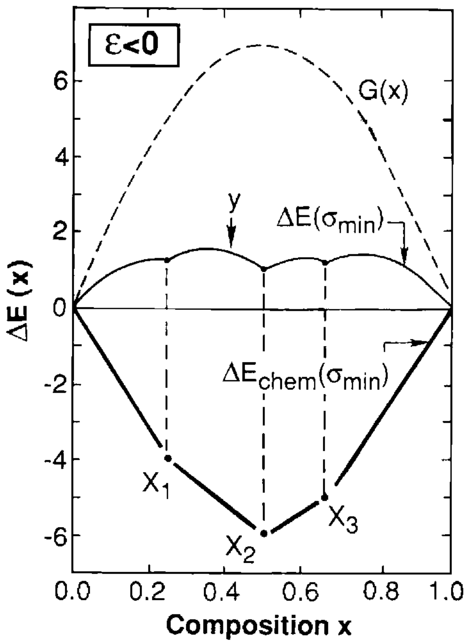

Fig. 3 Schematic plot of the chemical ground state line $\Delta E_{chem}(\sigma_{min})$, which is the second term in Eq. (22), the elastic energy $G(x)$, and their sum $\Delta E(\sigma_{min})$ Note that at compositions y between the vertex points of $\Delta E_{chem}(\sigma_{min})$, the system can lower its energy by local decomposition, whereas the vertex points X_1, X_2, and X_3 are locally stable with respect to decomposition and hence will produce metastable long-range ordering.

input to these calculations is the equation of states $\{\Delta E(V)\}$ of a set of ordered intermetallic A-B systems. These are determined from self-consistent local density calculations, as described above. As the next step, we wish to find the ground-state configuration that has the lowest $\Delta E(\sigma,V)$.

The ground state for a Hamiltonian as Eq. (12) or Eq. (22) is a classical problem in magnetism and in the theory of alloys. For fcc alloys, the most complete search for the ground state was given by Kanamori and Kakehashi (1977); for bcc, it was given by Finel and Ducastelle (1984).

At this point we should define what we understand by the ground state of the alloy. Let σ, α, and β be three configurations with concentrations of B atoms $x(\sigma)$, $x(\alpha)$, and $x(\beta)$ in the order

$$x(\alpha) \leqslant x(\sigma) \leqslant x(\beta). \qquad (24)$$

If $E(\sigma)$ is larger than the linear average of $E(\alpha)$ and $E(\beta)$, that is,

$$E(\sigma) > \frac{x(\sigma) - x(\beta)}{x(\alpha) - x(\beta)} E(\alpha) + \frac{x(\sigma) - x(\alpha)}{x(\beta) - x(\alpha)} E(\beta) \quad (25)$$

then configuration σ does not belong to the ground state because a mixture of the phases α and β would have a lower energy. A plot of the ground-state energy as a function of the concentration x has a similar characteristic shape shown schematically in the bottom part of Figure 3. It consists of straight line pieces between "breaking points," which correspond to some ordered (periodic) configurations of atoms. Any configuration σ could be represented in Figure 3 by a point $\{x(\sigma), E(\sigma)\}$. This point would be *above* the ground-state line (GSL) if Eq. (24) and Eq. (25) are satisfied for a certain pair α, β.

Though restricted, the Kanamori-Kakehashi study is very enlightening. For $0 \leqslant x \leqslant 0.5$ and any ratios $v_{2,2}/v_{2,4}$ and $v_{2,3}/v_{2,4}$, they found that, with the number of atoms per cell $\leqslant 16$, only 40 configurations can be ground states (i.e., breaking points of the GSL). These periodic structures have different numbers M of atoms in the unit cell. Table 1 shows the number of Kanamori-Kakehashi ground-state structures as a function of their unit cell sizes M. One sees that, in general, ground-state structures have rather small unit cells: only eight possible breaking points have unit cells with more than 12 atoms per cell (or 12 fcc sites). Moreover, configurations with large unit cells, though theoretically belonging to the GSL, might be very difficult to grow because they require a long-range correlation between atomic positions. For these two reasons it is practical to study the ground state, restricting ourselves to those configurations with unit cells of limited sizes.

Our calculation of the ground state then proceeds in two steps. First, we construct a file of all fcc-based and bcc-based configurations with unit cells smaller or equal to a certain maximum size (10–15 sites). In this file, for each configuration, we store the values of $\overline{\Pi}_F$ for the figures F of Figure 2. In the next section we describe a systematic procedure to construct this file, without missing any configuration, and without repetitions. Second, once the file is constructed, the ground state for a given set of interactions $\{v_F\}$ is found as follows:

1. For each configuration σ read $\{\overline{\Pi}_F\}$ from the file and calculate $E(\sigma)$.
2. Compare $E(\sigma)$ and $x(\sigma)$, according to Eqs. (24) and (25), with the configurations α and β that, up to this point, were found to be breaking points and are closest in concentration to σ.
3. If Eq. (25) is not satisfied for pairs α and β that satisfy Eq. (24), configuration σ is a new breaking point.
4. If σ is a new breaking point, scan the previously determined breaking points α and β to see whether any of them are now excluded from the GSL due to the introduction of σ.

CONSTRUCTING A CONFIGURATIONS FILE

Let $\mathbf{a}_1$, $\mathbf{a}_2$, and $\mathbf{a}_3$ be the unit vectors of the periodic configuration. Choosing the lattice parameter $a = 2$, the unit vectors are (l,m,n) with

$$l + m + n = \text{even (fcc)}, \qquad (26)$$

$$l,\ m,\ n = \text{all even, or all odd (bcc)}. \qquad (27)$$

For the fcc lattice itself, the unit vectors are $\mathbf{A}_1 = (0,1,1)$, $\mathbf{A}_2 = (1,0,1)$, and $\mathbf{A}_3 = (1,1,0)$. For the bcc lattice, they are $\mathbf{A}_1 = (-1,1,1)$, $\mathbf{A}_2 = (1,-1,1)$, and $\mathbf{A}_3 = (1,1,-1)$. The systematic generation of periodic configurations requires first a systematic generation of their triads of unit vectors $\{\mathbf{a}_i\}$. This is done as follows:

Table 1

Number of Kanamori-Kakehashi Ground-State Structures as a Function of Number of Atoms per Cell with Concentration $x \leqslant 0.5$

No. of Atoms/Cell *M*	No. of Kanamori-Kakehashi Structures
$\leqslant 2$	1
$\leqslant 4$	5
$\leqslant 6$	13
$\leqslant 8$	20
$\leqslant 10$	24
$\leqslant 12$	32
$\leqslant 16$	40

1. Require that for fcc

$$\mathbf{a}_1 \times \mathbf{a}_2 \cdot \mathbf{a}_3 = 2M. \tag{28}$$

where M is the number of fcc sites per cell (for bcc multiply M by 2 in this and subsequent formulae).

2. Require that

$$a_3^2 \geqslant a_2^2 \geqslant a_1^2. \tag{29}$$

3. Since adding or subtracting from $\mathbf{a}_2$ a multiple of $\mathbf{a}_1$ does not change the lattice, we require

$$\begin{gathered}(\mathbf{a}_2 \pm \mathbf{a}_1)^2 \geqslant a_2^2, \text{ or} \\ a_1^2 \geqslant 2\mathbf{a}_1 \cdot \mathbf{a}_2 \geqslant 0.\end{gathered} \tag{30}$$

4. One may add any integer combination of $\mathbf{a}_1$ and $\mathbf{a}_2$ to $\mathbf{a}_3$ without changing the lattice, so that we require

$$\mathbf{a}_3 = t\mathbf{a}_1 + u\mathbf{a}_2 + z\mathbf{a}_1 \times \mathbf{a}_2, \tag{31}$$

with

$$z = \frac{2M}{(\mathbf{a}_1 \times \mathbf{a}_2)^2} \tag{32}$$

and

$$-0.5 < t \leqslant 0.5 \tag{33a}$$

$$-0.5 < u \leqslant 0.5. \tag{33b}$$

One can then readily prove that

$$a_1^2 \leqslant (16\,M^2)^{1/3} \tag{34}$$

$$a_2^2 \leqslant \frac{a_1^2}{3} + \left[\frac{a_1^4}{9} + \frac{16\,M^2}{3\,a_1^2}\right]^{1/2} \tag{35}$$

$$a_3^2 \leqslant \frac{4\,M^2}{(\mathbf{a}_1 \times \mathbf{a}_2)^2} + \frac{a_1^2 + a_2^2 + 2\,\mathbf{a}_1 \cdot \mathbf{a}_2}{4}. \tag{36}$$

5. We can also make use of the rotational symmetry of the fcc (bcc) lattice. Choose $\mathbf{a}_1 = (l_1, m_1, n_1)$ so that Eq. (34) is satisfied and

$$l_1 \geqslant m_1 \geqslant n_1 \geqslant 0. \tag{37}$$

6. Choose $\mathbf{a}_2 = (l_2, m_2, n_2)$ so that Eqs. (30) and (35) are satisfied. Further, if $\mathbf{a}_1 \cdot \mathbf{a}_2 = 0$, choose $l_2 \geqslant 0$; if l_2 is also zero, choose $m_2 \geqslant 0$; if m_2 is also zero, choose $n_2 > 0$. Further, if $m_1 = 0$, choose $m_2 \geqslant 0$, and if $n_1 = 0$, choose $n_2 \geqslant 0$. Further, if $l_1 = m_1$, choose $l_2 \geqslant m_2$, and if $m_1 = n_1$, choose $m_2 \geqslant n_2$.
7. Choose $\mathbf{a}_3 = (l_3, m_3, n_3)$ so that Eqs. (36), (31), (32), and (33) are satisfied.

The set of triads generated according to the recipes above still contains repetition—that is, triads generating lattices related by symmetry—despite all the requirements that were set. So, starting from $M = 2$, we generate a file of triads, and for each new triad we verify that it is not equivalent to a previous one already in the file. This is done in the following way. Let $\mathbf{p}_1$, $\mathbf{p}_2$, and $\mathbf{p}_3$ be the unit vectors of a previous triad. If the triad $\{\mathbf{a}_j\}$ is equivalent to $\{\mathbf{p}_i\}$ then it is possible to find a point group operation R so that $\mathbf{p}_i$ is an integer combination of the rotated $\mathbf{a}_j$

$$\mathbf{p}_i = \sum_j l_{ij} R \mathbf{a}_j. \tag{38}$$

Letting $\{\mathbf{g}_k\}$ be the reciprocal vectors of $\{\mathbf{a}_j\}$, or

$$\mathbf{g}_k \cdot \mathbf{a}_j = \delta_{jk}, \tag{39}$$

for instance

$$\mathbf{g}_3 = \frac{\mathbf{a}_1 \times \mathbf{a}_2}{(\mathbf{a}_1 \times \mathbf{a}_2) \cdot \mathbf{a}_3}, \tag{40}$$

we say that $\{\mathbf{a}_j\}$ is not equivalent to any previous $\{\mathbf{p}_i\}$ if there is no point group operation R for which

$$\mathbf{p}_i \cdot R\mathbf{g}_k = \text{integer} \tag{41}$$

for all i and k.

Once a new triad has been found (defining a unit cell with M fcc sites), we must study the 2^M configurations obtained by occupying the M sites with atoms A or B. This study begins by finding the Cartesian coordinates of the M sites.

Let $\{\mathbf{A}_i\}$ be the primitive unit vectors of the fcc (or bcc) lattice itself. (Do not confuse it with the primitive unit vectors $\{\mathbf{a}_i\}$ of the periodic configuration to be constructed, which is the triad just found.) The M sites of the unit cell of the configuration (basis vectors $\mathbf{b}_i$) are integer combinations of the vectors $\mathbf{A}_j$

$$\mathbf{b}_i = \sum_j l_{ij} \mathbf{A}_j;\ (i = 1,2, \ldots M \text{ and } j = 1,2,3). \tag{42}$$

Now, the unit vectors of the configuration are themselves integer combinations of $\mathbf{A}_j$

$$\mathbf{a}_i = \sum_j m_{ij} \mathbf{A}_j \tag{43}$$

then

$$\mathbf{b}_i = \sum_{j,k} l_{ij} m_{jk}^{-1} \mathbf{a}_k. \tag{44}$$

Now, the determinant of the matrix m is equal to the number M of sites

$$2M = (\mathbf{a}_1 \times \mathbf{a}_2) \cdot \mathbf{a}_3 = \sum_{j,k,l} m_{1j} m_{2k} m_{3l} (\mathbf{A}_j \times \mathbf{A}_k) \cdot \mathbf{A}_l = \sum_{j,k,l} m_{1j} m_{2k} m_{3l} 2\epsilon_{jkl} = 2\ \det[m]. \tag{45}$$

One sees that in adding to any of the integers l_{ij} in Eq. (44) a multiple of M, one is adding to $\mathbf{b}_i$ an integer combination of the unit vectors of the configuration $\{\mathbf{a}_i\}$, and therefore pointing to a position in the same sublattice, but *outside* the unit cell. Hence, the search for the basis vectors $\{\mathbf{b}_i\}$ can be made by scanning the integers l_{ij} in the range

$$0 \leq l_{ij} \leq M - 1. \tag{46}$$

Of course, in finding a new basis vector $\mathbf{b}_i$, we must verify that it is not pointing to a site differing from a previous basis vector $\mathbf{b}_p$ by an integer combination of the unit vectors, or a site in a sublattice already found. In other words, it is necessary that at least for one of the reciprocal vectors $\mathbf{g}_j$

$$(\mathbf{b}_i - \mathbf{b}_p) \cdot \mathbf{g}_j \neq \text{integer}. \tag{47}$$

Having established the basis vectors, the M sublattices

$$\mathbf{b}_i + \sum_j J_{ij} \mathbf{a}_i, \tag{48}$$

with J_{ij} = integer, are occupied with atoms A or B in 2^M different ways. Each configuration is represented by a number B

$$0 \leq B \leq 2^M - 1 \tag{49}$$

written as a binary. For instance, for $M = 6$, the configuration $B = 13$ is 001101 meaning *AABBAB*, or that the second, fifth, and sixth sublattices are occupied by A, while the first, third, and fourth sublattices have atoms B. The corresponding spins are -1, -1, 1, 1, -1, 1. We store in the file the configurations with concentration x of atoms B $x \leq 0.5$; the other configurations are discarded. Since the origin can be placed anywhere, we also require that the spin of the first sublattice is +1 (atom B).

After occupying the M sublattices with atoms A or B, it may happen that the translational symmetry of the resulting configuration is larger than what was assumed by the unit vector $\{\mathbf{a}_1\}$. For instance, in an fcc-based configuration with unit vectors $\mathbf{a}_1 = (2,0,0)$, $\mathbf{a}_2 = (0,2,0)$, and $\mathbf{a}_3 = (0,0,2)$ there are $M = 4$ sublattices with bases $\mathbf{b}_1 = (0,0,0)$, $\mathbf{b}_2 = (1,1,0)$, $\mathbf{b}_3 = (1,0,1)$, and $\mathbf{b}_4 = (0,1,1)$. If one occupies $\mathbf{b}_1$ and $\mathbf{b}_2$ with A's, $\mathbf{b}_3$ and $\mathbf{b}_4$ with B's, we obtain the CuAuI configuration with just two atoms per cell, and not the four sites originally assumed. These configurations with increased translational symmetry are discarded because they had been considered previously when calculating the configurations with smaller values of M. The extra-translational symmetry corresponds to a translation vector that belongs to the full fcc translation group but is left out in the translation group generated by $\{\mathbf{a}_i\}$. Then the extra-translation vector must correspond to one of the basis vectors $\{\mathbf{b}_i\}$. The criterion is the following: a translation $\mathbf{b}_i$ also belongs to the symmetry group of the configuration if, for all basis vectors $\mathbf{b}_j$,

$$\hat{S}(\mathbf{b}_j + \mathbf{b}_i) = \hat{S}(\mathbf{b}_j). \qquad (50)$$

In other words, $\mathbf{b}_j + \mathbf{b}_i$ and $\mathbf{b}_j$ have the same spin, or the same atom. If Eq. (50) is satisfied for all j and a certain i, the configuration has higher translational symmetry than assumed and must be discarded.

Thus, given a triad of unit vectors, the 2^M configurations are submitted to the three tests above: namely, $x \leq 0.5$; atom B at the origin; and no extra-translational symmetry. For those configurations σ that pass these tests, we calculate the lattice averaged spin product $\overline{\Pi}_F(\sigma)$ according to Eq. (11). The sum in Eq. (11) was taken over all space group operations of the original fcc lattice. However, this is not needed here because the configuration σ has a definite translation group generated by the triad of unit vectors $\{\mathbf{a}_i\}$, and so we just sum over the factor group made of the 48 rotations and the M translations with vectors $\{\mathbf{b}_j\}$. Accordingly, the denominator becomes 48 M and not 48 N. Rotating and translating these vertices presents no problem. After the operation R on a vertice $\mathbf{v}$, the sublattice i of $R\mathbf{v}$ is identified by verifying that

$$(R\mathbf{v} - \mathbf{b}_i) \cdot \mathbf{g}_j = \text{integer} \qquad (51)$$

for all J. Thus, one knows the spin of the operated vertices and can make the product $\Pi_{RF}(\sigma)$ and calculate the average $\overline{\Pi}_F(\sigma)$.

Finally, very frequently two configurations with the same triad of unit vectors but with different occupation of B atoms will be symmetry-related. Since the table of $\overline{\Pi}_F$ distinguishes two symmetry-unrelated configurations, according to Eq. (12), we must determine if the configuration just generated has a set of $\overline{\Pi}_F$ different from those of the configurations previously found. If the set coincides with that of a previous configuration, the new configuration must be discarded to avoid repetition. Because we are working with only eight figures, and not an infinite set of figures, we might be making a bit of overelimination, for it happens that two symmetry-unrelated configurations with the same triad of unit vectors might have equal sets of eight average $\overline{\Pi}_F$. This overelimination is of no consequence if the interactions v_F are also restricted to the eight figures.

In Table 2 we show the number of configurations for different values of the cell size M. The number increases very fast with M, so that the computing time and the storing of $\{\overline{\Pi}_f\}$ file become enormous if M is taken beyond 10. Fortunately, this calculation needs to be done only once for fcc and bcc symmetries. On the other hand, as exemplified by the Kanamori-Kakehashi study, and explained in the preceding section, the upper limit $M \sim 10$ already includes the most important configurations and allows a realistic description of the GSL. In our actual calculations we used $M = 15$ so that about $2^{15} = 32{,}768$ possible structures are examined for each compound.

Results

Referring above to the section Statement of the Physical Problem, we have carried through steps 1 through 4 for seven semiconductor alloys. The phase diagram calculations were done using CVM (Kikuchi, 1951, 1974) with up to four (folded) neighbor interactions and four body terms (Ferreira, Wei, and Zunger, 1989). We next discuss the salient features of the results.

THE QUANTUM-MECHANICAL INTERACTION ENERGIES

Using the LAPW calculated equations of state $\{\Delta E(s,V)\}$ for the eight special periodic structures (Fig. 1) and Eq. (16), we obtain the volume-dependent interaction energies depicted in Figure 4 for three alloy systems. These show the following:

1. $J_0(V)$ and $J_1(V)$ have a significant volume dependence; $J_0(V)$ is much larger at $x = ½$ than all $J_{F\neq 0}$.
2. Three- and four-body terms are rather small for semiconductor alloys.
3. Regarding the pair ($k = 2$) interactions $J_{2,m}$ between m neighbors, we find $J_{2,1}$ (first-neighbor pair) to be dominant. Yet the fourth-neighbor interaction $J_{2,4}$ is larger than the second-neighbor ($J_{2,2}$) and third-neighbor ($J_{2,3}$) pair interactions. This result is found to hold for all eight semiconductor systems. This nonmonotonicity of $J_{2,m}$ with m

$$|J_{2,1}| > |J_{2,4}| > |J_{2,2}|, |J_{2,3}| \qquad (52)$$

serves as a warning against simple truncation of the energy expansion, Eq. (12), on the basis of a hierarchy in m.

FORMATION AND MIXING ENTHALPIES

Figure 5 shows the reduced mixing enthalpy ("interaction parameter")

$$\hat{\Omega}_H(x,T) = \Delta H(x,T)/x(1 - x) \qquad (53)$$

for the disordered alloy at two temperatures (solid lines), and the analogous quantity (reduced formation enthalpy) for the ordered compounds s at $T = 0$

$$\hat{\Omega}_s(X_s, T = 0) = \Delta E(s,V_s)/X_s(1 - X_s), \qquad (54)$$

depicted as solid diamonds.

The basic features of our results in Figure 5 are as follows. First, for size-mismatched alloys, the (201)-type structures such as chalcopyrite have a lower enthalpy than the disordered alloy. We will see below that this leads to *metastable long-range ordering of size-mismatched*

Table 2

Number of Configurations Having Different Triads of Unit Vectors and/or Different Sets of Eight $\overline{\pi}_F$ in the fcc and bcc Systems as a Function of Number of Atoms per Cell

No of Atoms/Cell M	No. of fcc-Based Configurations with $x \leq 0.5$	No. of bcc-Based Configurations with $x \leq 0.5$
1	1	1
2	2	2
3	3	3
4	12	12
5	14	14
6	49	50
7	52	52
8	225	228
9	239	237
10	660	653

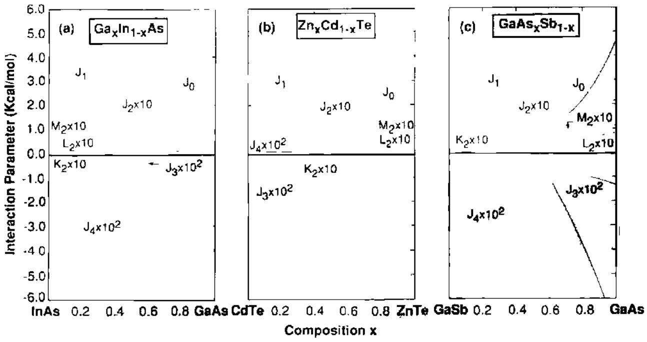

Fig. 4 LAPW-calculated interaction energies from Eq. (16) for three semiconductor alloys

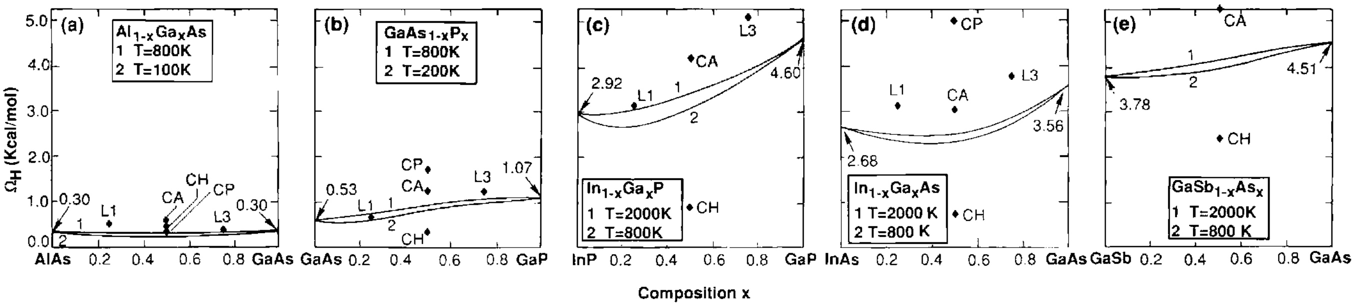

Fig. 5 Calculated reduced enthalpy for the disordered alloy (solid lines), see Eq. (53), and for ordered compounds (diamonds), see Eq. (54)

semiconductor alloys, as observed in liquid-phase epitaxy growth (Nakayama and Fujita, 1986) of $In_{1-x}Ga_xAs$ and in vapor growth (Jen, Cherng, and Stringfellow, 1986, 1987) of $GaSb_{1-x}As_x$.

Second, for size-matched alloys, the disordered alloy has a lower enthalpy than any of the simple ordered structures studied; hence, *no thermodynamically mandated ordering is expected in size-matched semiconductor alloys.* The CuAuI-like ordering observed by Kuan et al. (1985) in $Al_{1-x}Ga_xAs$ is likely to be surface-induced.

Third, the CuPt ordering recently observed in epitaxial growth of size-mismatched semiconductor alloys (see Fig. 1) is characterized by a considerably higher enthalpy than the disordered alloy; hence, *bulk effects produce neither stable nor metastable CuPt ordering in size-mismatched semiconductor alloys.*

Fourth, $\hat{\Omega}(x,T)$ has a significant composition dependence neglected by most phenomenological models (e.g., Panish and Ilegems, 1972). Note that when B is the smaller of the two atoms in $A_{1-x}B_x$, we find that $\hat{\Omega}(0) < \hat{\Omega}(1)$. This reflects the fact that more energy is required to incorporate a large atom A in a small host crystal B (i.e., $x \rightarrow 1$) than to incorporate a smaller atom B in a large host crystal A (i.e., $x \rightarrow 0$).

PHASE DIAGRAMS

Figures 6 and 7 depict the calculated phase diagrams of the eight alloy systems in the high-temperature range where disordered alloys exist. The calculations show the binodal ("miscibility") line as well as the spinodal. The binodal is the line in the (x,T) plane where the A-rich and B-rich disordered phases have equal chemical potentials μ. The spinodal line describes the limit of metastability of the disordered phase when $d^2F/dx^2 = d\mu/dx = 0$, F being the free energy. In all cases, we find that the thermodynamically stable ground state corresponds to phase separation. The phase diagrams are generally asymmetric with respect to $x = \frac{1}{2}$.

Experimental data on the solid-state part of semiconductor alloy phase diagrams are fragmentary: although detailed data exist on the high-temperature liquidus and solidus lines, the low atomic diffusion constants at lower temperatures make such studies in solid semiconductors difficult. The recent data of Ishida et al. (1988) for $GaSb_{1-x}As_x$ shown in Figure 6 and exhibiting close agreement with the calculation are a notable exception.

METASTABLE ORDERED PHASES

The persistently lower formation enthalpy of the ABC_2 chalcopyrite structure relative to the disordered phase in size-mismatched alloys (Fig. 5) suggests the possibility of metastable long-range ordering into this structure. We calculated the temperature limit of stability for this phase, according to $\partial^2F/\partial x^2 = 0$. The results are summarized in Table 3. At thermodynamic equilibrium, the system phase separates below T_{MG} into AC-rich plus BC-rich mixtures, while above T_{MG} a homogeneous alloy persists. If, however, phase separation is kinetically inhibited, metastable long-range ordering will persist below T_c (Table 3). These structures are metastable in a very specific manner: they are more stable below T_c than the homogeneous disordered alloy, but unstable with respect to phase separation. Note that other ordered structures such as CuPt or CuAuI are not metastable: they are *unstable* with respect to both disordering

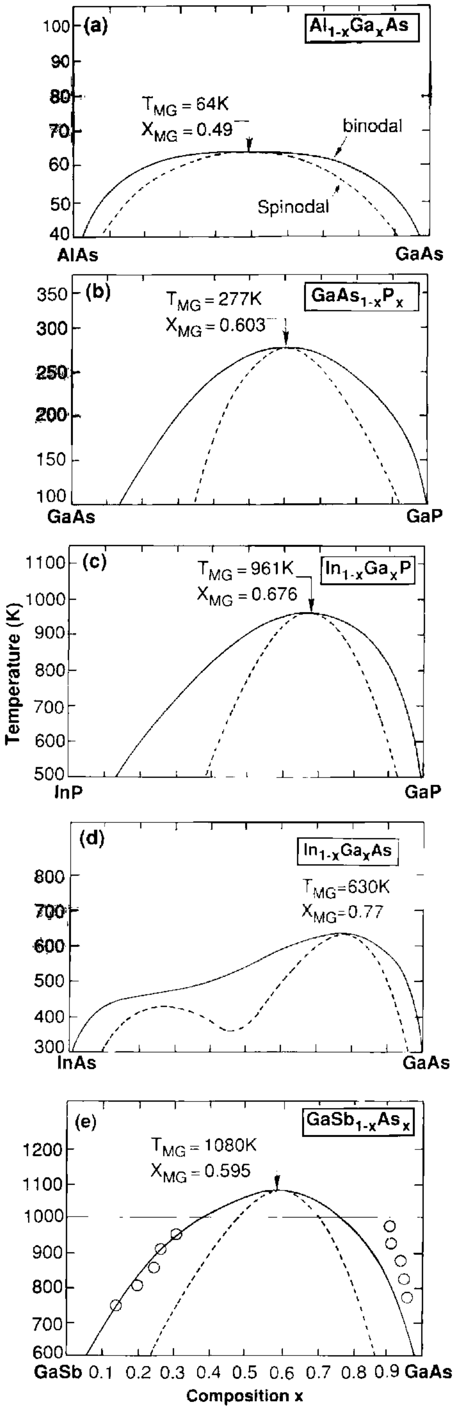

Fig. 6 Calculated phase diagrams for the III-V alloys (a) $A\ell_{1-x}Ga_xAs$, (b) $GaAs_{1-x}P_x$, (c) $In_{1-x}Ga_xP$, (d) $In_{1-x}Ga_xAs$, and (e) $GaSb_{1-x}As_x$ The solid (dashed) lines give the binodal (spinodal) lines. Low-temperature ordered phases are not shown (given in Table 5). The arrows point to the maximum miscibility gap (MG) temperatures and compositions. The circles in part (e) are the recent experimental data of Ishida et al. (1988); the horizontal line represents the peritectic line.

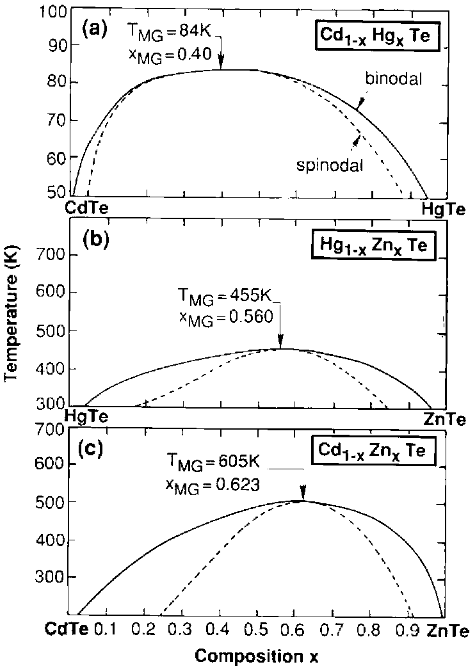

Fig. 7 **Calculated phase diagrams for the II-VI alloys (a) $Cd_{1-x}Hg_xTe$, (b) $Hg_{1-x}Zn_xTe$, and (c) $Cd_{1-x}Zn_xTe$**

and phase separation. This result highlights the significance of interactions beyond first nearest neighbors: retaining interactions only up to first neighbors (J_2) leads to a degeneracy of the energies of the CuAuI and chalcopyrite structures.

COMPARISON OF MONTE CARLO AND CVM SOLUTIONS TO THE ISING HAMILTONIAN

A distinct advantage of the representation of the Ising Hamiltonian in Eq. (22) is its amenability to Monte Carlo simulations, which are considerably more difficult when J_F are functions of volume. To assess the validity of our folding method whereby second, third, and fourth neighbor pair interactions are renormalized into effective nearest-neighbor interactions $\tilde{J}(x,V)$, we compared the CVM solution of this Ising Hamiltonian, Eq. (22), including folding, to a Monte Carlo solution of the full (unfolded) Hamiltonian.

For simplicity, we select in Eq. (22) $G(x) = \tilde{\Omega}\, x(1-x)$ and remove the three- and four-body terms, that is, $v_{3,1} = v_{4,1} = 0$. These simplifications lead to a phase diagram that is symmetric about $x = ½$ and the two-phase equilibrium occurs at the chemical potential $\mu = 0$. Thus, the search for the phase equilibrium line in the (μ,T) plane (a very time-consuming step in Monte Carlo) is simplified. The parameters used, appropriate to $GaSb_{1-x}As_x$, are (in meV)

Table 3

Calculated Miscibility Gap Temperatures T_{MG}, the Composition $x_{MG} = X(T_{MG})$, and Interaction Parameters $\hat{\Omega}_H(x)$ of Eq.(53) at $T = 800$ K and the Spinodal Ordering Temperatures for a Number of Metastable Long-Range Ordered Phases

	T_{MG} (K)	x_{MG}	Interaction Parameters (kcal/mol)			Ordering Temperature (K)			
			$\hat{\Omega}_H$ (0)	$\hat{\Omega}_H$ (1/2)	$\hat{\Omega}_H$ (1)	T_{CH}	T_{C1}	T_{C2}	T_{F1}
$A\ell_{1-x}Ga_xAs$	64	0.49	0.30	0.30	0.30	0	0	0	0
$GaAs_{1-x}P_x$	277	0.603	0.53	0.86	1.07	75	91	67	80
$In_{1-x}Ga_xP$	961	0.676	2.92	3.07	4.60	463	305	215	450
$GaSb_{1-x}As_x$	1,080	0.595	3.78	3.96	4.51	285	170	139	—
$In_{1-x}Ga_xAs$	630	0.770	2.68	2.35	3.56	320	167	136	80
$Cd_{1-x}Hg_xTe$	84	0.40	0.45	0.38	0.31	0	0	0	0
$Hg_{1-x}Zn_xTe$	455	0.560	2.13	1.88	2.15	256	135	87	200
$Cd_{1-x}Zn_xTe$	605	0.623	2.24	2.29	2.87	270	158	117	205

Phases are defined in Figure 1 and Table 5.

$$\begin{aligned} v_{2,1} &= 6.6167,\ v_{2,2} = 1.7588, \\ v_{2,3} &= 0.4938,\ v_{2,4} = 4.0018, \\ v_{0,1} &= -\sum_{m} D_{2,m} v_{2,m} = -74.913, \end{aligned} \qquad (55)$$

and $\bar{\Omega}$ = 948.5059 meV (four atoms).

The Monte Carlo runs were made using single spin-flip kinetics (Styre, Phani, and Lebowitz, 1986). We used a cell of 12^3 = 1,728 fcc sites, 100 flip attempts per site, to reach steady state and 400 attempts per site to collect data. The acceptance ratio, which is defined as the fraction of successful flip attempts, was minimum at 700 K, when it attained a value of 19%, and it increased rapidly as the temperature was raised.

The results are presented in Figure 8. The binodal points were determined by starting from a random sample with x = 0.99, letting it stabilize, and collecting data at μ = 0. Above 850 K and below T_{MG}, the spin-flip process led to a two-phase system, and the sample oscillated between these two phases in equilibrium. Thus, it was impossible to determine accurately the equilibrium concentration of each phase. Although the oscillations of x are large, we observed that the probability of finding pairs AB, which is equal in the two phases, had small oscillations. Therefore, we used this fact to find the critical temperature. Figure 8b presents the interaction parameter at 1,000 K. In all cases, the dots, bars, or rectangles are in size equal to or greater than the standard deviation.

Figure 8 shows an excellent agreement between the phase diagram (9a) and mixing enthalpy (8b) obtained from Monte Carlo and CVM solutions. We have also included for comparison results obtained by the mean-field Bragg-Williams (BW) approach (Bragg and Williams, 1934) in which all correlations are neglected. We conclude that our tetrahedron CVM with folded distant-pair interactions in no way worsens the good agreement between standard CVM and Monte Carlo. Thus, the folding method opens the way to the inclusion in CVM of more realistic and complicated Hamiltonians.

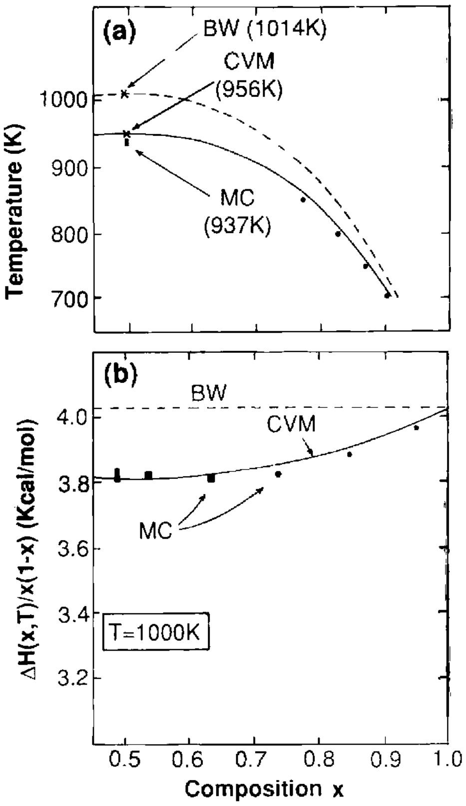

Fig. 8 (a) Phase diagram (binodal) using CVM with folded distant-neighbor interaction (full line), Bragg-Williams (BW, dashed line), and Monte Carlo (MC, dots and bar) method The Hamiltonian is given in Eq. (22) with parameters of Eq. (55). **(b) The normalized mixing enthalpies for these three models** The rectangles depicting Monte Carlo results indicate the size of the standard deviation in x and $\Delta H/x(1-x)$. The standard deviation is smaller than the sizes indicated by the solid circles.

THE SEARCH FOR GROUND STATES

The use of the energy expansion in terms of multisite interaction energies and the determination of the interaction energies permit us to capitalize on our method to find the ground states supported by this Hamiltonian. The stability analysis is most simply made in the (ϵ, G) formalism, where the configuration σ has the energy given by Eq. (22). We will refer to the second term of this equation as the "chemical" energy $\Delta E_{chem}(\sigma)$. To establish the stability conditions, we proceed in two steps.

First, we compare structures with fixed composition x and search for the lowest energy at each x. In this case, the term $G(x)$ is irrelevant because it is common to all structures at the same x. The GSL of the chemical energy $\Delta E_{chem}(\sigma_{\min})$ is obtained in the way outlined above in the section Convergence of the Cluster Expansion.

In the second step we consider the effect of the elastic energy $G(x)$ on the decomposition of a phase $\alpha\beta$ into two phases of different compositions, for example,

$$2\alpha\beta(x) \rightleftarrows \alpha(x + \omega) + \beta(x - \omega), \tag{56}$$

where ω is an infinitesimal composition change. Figure 3 shows schematically $G(x)$, and the sum $\Delta E(\sigma_{\min})$ of $G(x)$ with the GSL $\Delta E_{chem}(\sigma_{\min})$ as a solid line. For size-mismatched semiconductors, the positive elastic energy $G(x)$ overwhelms the negative chemical energy; since the sum of these two contributions $\Delta E(\sigma_{\min})$ is nonnegative for all x's, the ground state at $T = 0$ corresponds to a mixture of the pure binary constituents. However, local minimum can exist. This can be seen by considering a com-

Table 4

Ordered Configurations Corresponding to Vertices in the Ground-State Line of Chemical Energy $\Delta E_{chem}(\sigma)$

x	Our Symbol	Kanamori Symbol	Superlattice Description	Atoms per Cell	GaSb GaAs	GaP InP	GaP GaAs	InAs GaAs	HgTe ZnTe	CdTe ZnTe
1/13		[0,0,0,0;1/13]	(12,1) [9,3,1]	13	x			x		
1/9		[0,1,0,0;1/9]	(8,1) [3,1,0] or [9,3,1]	9		x	x	x	x	x
1/7		[0,0,3,0;1/7]	(6,1) [5,3,1]	7	x					
1/5		[0,1,4,0;1/5]	(4,1) [2,1,0]	5	x	x	x	x	x	x
1/4		[1/2,1,5,0;1/4]	(4,1,2,1) [2,1,0]	8	x	x	x	x	x	x
2/7		[3/4,1,21/4,1/2;2/7]	(3,1,4,1,3,2) [7,5,1]	14	x			x		
		[1/2,3/2,5,1;2/7]	(3,1,2,1) [2,1,0]	7		x	x		x	x
1/3	*C1*	[1,1,6,1;1/3]	(2,1) [1,1,0] or [2,1,0]	3	x					
		[1,3/2,11/2,1;1/3]	(4,1,1,1,2,1,1,1) [3,1,0]	12		x	x	x	x	x
2/5		[3/2,3/2,6,3/2;2/5]	(3,2) [2,1,0]	5	x	x		x		
5/12		[8/5,9/5,32/5,8/5;5/12]	(3,1,2,2,2,2) [3,2,0]	12		x	x		x	x
1/2	*CH*	[2,2,8,2;1/2]	(2,2) [2,1,0]	4	x	x	x	x	x	x

All configurations with up to 15 atoms per cell were considered. These configurations are superlattices with alternating planes (*p*,*q*,*r*, . . .), i.e., *p* planes of *A*, followed by *q* planes of *B*, *r* planes of *A*, etc., along the direction [*l*,*m*,*n*]. An "x" symbol in the last six columns indicates that the corresponding phase is a ground state.

position y between two vertices of the GSL (say, 1 and 2 in Fig. 3). In this case the energy change associated with reaction (56) is purely elastic, that is,

$$\delta\Delta E = G(y+\omega) + G(y-\omega) - 2G(y) = \omega^2 \frac{d^2G}{dx^2}\Big|_y. \tag{57a}$$

Since by Eq. (20) $d^2G/dx^2 = -Z(x)$ where $Z(x) > 0$ by Eq. (21b), this energy change must be negative, that is,

$$\delta\Delta E = -\omega^2 Z(y) < 0, \tag{57b}$$

and the reaction (56) proceeds to the right (decomposition). This process can continue until one reaches a composition y corresponding to a vertice in the GSL surrounded by two minima (e.g., vertex 2 surrounded by vertices 1 and 3 in Fig. 3). Now the energy change associated with reaction (56) has both elastic and chemical contributions. By Eq. (57) we have

$$\delta\Delta E = -\omega^2 Z(y) + \omega\left\{\frac{\epsilon^{(3)} - \epsilon^{(2)}}{X_3 - X_2} - \frac{\epsilon^{(2)} - \epsilon^{(1)}}{X_2 - X_1}\right\}. \tag{58}$$

Since the second term ("chemical") is positive and linear in the concentration fluctuation ω, it will overwhelm the elastic term (quadratic in ω) for small ω. In this case $\delta\Delta E$ is positive and reaction (56) proceeds to the left: compound formation is favored. *Hence, the local minima of* $\Delta E(\sigma_{min})$ (Fig. 3) *correspond to metastable long-range ordering.* We conclude that at a general composition x, phase separation will occur until a special composition X_2 is encountered, at which point $\Delta E(X_2)$ becomes locally stable against composition fluctuations. In perfect equilibrium at X_2, the system will overcome the barriers evident in Figure 3 and produce the true phase-separated ground state. However, at sufficiently low temperatures the system cannot surmount these barriers and will exhibit long-range ordering in the phases shown in Table 4. This demonstrates that metastable long-range ordering found in our phase diagram calculations is a consequence of the coexistence of negative chemical energies with (larger), positive elastic energies.

Having identified the ground-state structures, we note that it remains to be seen whether the stability limit temperature given by $d^2F/dx^2 = 0$ is sufficiently high to allow growth of these ordered phases. For this purpose, we constructed a CVM-correlation-function computer program able to calculate the free energy of any fcc-based structure specified by its unit vectors. The input to the program is only the triad of unit vectors and the occupation (with A or B) of its sublattices. The program itself generates the space group, determines the independent figures, finds the Kikuchi coefficients (1951, 1974) for the CVM entropy expansion using Barker's procedure (1953), finds the linear relations between reduced density matrix elements and correlation functions, and determines how the non-first-neighbor pair correlations decouple into products of point figure correlations. Application of this procedure to the ground-state structures of Table 4 provides their free energies $\Delta F(x,T)$, from which the stability limit is calculated.

In Table 5, we present the stability limit temperature for phases belonging to the GSL of GaSbAs. We see that these stability temperatures are well below current growth temperatures.

Conclusion

Our study suggests that the thermodynamic properties of bulk isovalent zincblende semiconductor alloys can be quantitatively understood in terms of a general Ising model with up to fourth-neighbor interactions and that the LDF forms are adequate basis for self-consistently describing those interactions. The global trends can be understood by separating in Eq. (22) the excess enthalpy $\Delta H(x,T)$ into a volume-dependent (or composition-dependent) term $G(x)$, reflecting microscopic size mismatch, and a sum over volume-independent configurational (or substitutional) energies ϵ, reflecting events at constant molar volume, that is, sublattice relaxation and charge redistribution. The alloys studied then separate naturally into two groups.

One group consists of size-matched alloys ($A\ell_{1-x}Ga_xAs$ and $Cd_{1-x}Hg_xTe$). Here, $G(x) \cong 0$, and owing to negligible sublattice relaxation and unfavorable charge redistribution, the substitutional energies ϵ are (slightly) positive. This leads to the following characteristics.

First, the disordered alloy has a lower excess enthalpy than any of the short-period ordered structures. Hence, these systems will disorder above T_{MG} and

Table 5

Limiting Temperature T_c of Stability for Some GaSbAs Phases Belonging to the Ground-State Line of Chemical Energies

x	Our Symbol	Kanamori Symbol	Atoms per Cell	Independent Figures	T_c (K)
1/5		[0,1,4,0;1/5]	5	2Q + 3T + 3P1 + 2D + 3P2 + 3P3 + 2P4	123
1/4		[1/2,1,5,0;1/4]	8	5Q + 12T + 14P1 + 4D + 10P2 + 10P3 + 6P4	137
1/3	*C*1	[1,1,6,1;1/3]	3	2Q + 4T + 4P1 + 2D + 3P2 + 3P3 + 3P4	153
2/5		[3/2,3/2,6,3/2;2/5]	5	3Q + 6T + 6P1 + 3D + 6P2 + 6P3 + 5P4	172
1/2	*CH*	[2,2,8,2;1/2]	4	1Q + 2T + 4P1 + 2D + 3P2 + 3P3 + 3P4	287
3/5		[3/2,3/6,6,3/2;3/5]	5	3Q + 6T + 6P1 + 3D + 6P2 + 6P3 + 5P4	178
2/3	*C*2	[1,1,6,1;2/3]	3	2Q + 4T + 4P1 + 2D + 3P2 + 3P3 + 3P4	165
3/4		[1/2,1,5,0;3/4]	8	5Q + 12T + 14P1 + 4D + 10P2 + 10P3 + 6P4	145
4/5		[0,1,4,0;4/5]	5	2Q + 3T + 3P1 + 2D + 3P2 + 3P3 + 2P4	140

Calculations were made with Eq.(22). We characterize each structure by the number and type of independent figures appearing in it. Here, Q means a tetrahedron, T a triangle, P1 a first-neighbor pair, D a point, and P2, P3, and P4 second-, third-, and fourth-neighbor pairs.

phase-separate into their constituents below it. No metastable long-range ordering occurs. Second, above T_{MG} the systems exhibit enhancement in the populations of the pure A_4 and B_4 cluster and a depletion of the mixed clusters ("clustering"), again reflecting $\epsilon > 0$. Finally, the mixing enthalpies are small and positive, reflecting $G \simeq 0$ and $\epsilon > 0$.

The other group consists of size-mismatched alloys ($GaAs_{1-x}P_x$, $In_{1-x}Ga_xP$, $In_{1-x}Ga_xAs$, $GaSb_{1-x}As_x$, $Cd_{1-x}Zn_xTe$, and $Hg_{1-x}Zn_xTe$). Here, $G(x) > 0$ owing to the *A*-*B* size mismatch, yet $\epsilon < 0$, predominantly because of an effective sublattice relaxation that leads to bond alternation and a partial accommodation of strain. This results in the following characteristics.

First, like size-matched alloys, size-mismatched alloys have $\Delta H(x,T) > 0$; hence, at $T = 0$ they will phase-separate when perfect equilibrium is achieved. However, if phase separation is slow, long-range ordering will occur in the structures identified in Table 4 at the temperatures predicted in Table 5. These special atomic arrangements have a lower enthalpy than does the disordered alloy of the same composition. These conclusions pertain to bulk growth (e.g., liquid phase epitaxy, or other melt techniques), since we have addressed in this work the thermodynamics of three-dimensionally coordinated atoms. Growth techniques involving a free surface (e.g., molecular-beam epitaxy) would have a different thermodynamics owing to the lower symmetry (e.g., surface clusters are likely to have different energies than clusters surrounded by atoms in all three directions). Indeed, in the presence of surface reconstruction effects, the energy-minimizing structure can be qualitatively different from that obtained by minimizing the bulk energy. To the extent that coverage of the surface freezes in the surface-stable structure, it could persist metastably to macroscopic dimensions. The fact that growth techniques that involve free surfaces exhibit CuPt ordering (Fig. 1) is most likely a reflection of this surface thermodynamic effect.

Second, above T_{MG}, lattice-mismatched systems will exhibit an excess of the mixed (A_3B, A_2B_2, and AB_3) clusters and a deficiency in the "pure" (A_4 and B_4) clusters ("anticlustering").

Third, their excess enthalpies largely reflect strain effects; hence, they scale approximately with the relative size mismatch $|a_A - a_B|/|a_A + a_B|$. These enthalpies are temperature-dependent owing to the pronounced temperature dependence of the cluster probabilities.

We conclude by contrasting our conclusions with those suggested by other alloy models. In classic models, based on *constant* interaction energies, alloys are broadly classified into two groups.

One group, alloys for which $\Delta H(x,T)$ in the disordered phase is known to be positive, are said to be characterized by repulsive interactions. This is said to lead to clustering in the disordered phase and, at sufficiently low temperatures, to phase separation. Repulsive interactions and long-range ordering are taken to be mutually exclusive. All isovalent semiconductor alloys are said to belong to this class.

The other group, alloys for which $\Delta H(x,T)$ in the disordered phase can be negative, are said to be characterized by attractive interactions. This is expected to lead to anticlustering in the disordered phase and to long-range order at sufficiently low temperatures.

Our work shows that this classification is false: alloys with $\Delta H(x,T) > 0$ (all isovalent semiconductors) can show clustering and phase separation (when size-matched) or anticlustering and metastable long-range ordering (when size-mismatched). This reflects the fact that there are two distinct physical sources to $\Delta H > 0$: $G(x)$ and ϵ, which control different aspects of the thermodynamics.

ACKNOWLEDGMENT

This work was supported by the Office of Energy Research, Division of Material Sciences, Office of Basic Energy Sciences (OER-BES) of the U.S. Department of Energy, under contract DE-AC02-77-CH00178. We are also grateful for the OER-BES "Grand Challenge" grant of computer time that made this work possible.

BIOGRAPHIES

L. G. Ferreira received his Ph.D. from the Massachusetts Institute of Technology in 1964. He has been a professor of physics at the Institute of Physics, University of São Paulo, Brazil, for the last 25 years. He is now at Campinas, Unicamp, Brazil. He spent a sabbatical year at the Solar Energy Research Institute in 1986 and has visited there every year since.

S.-H. Wei received his Ph.D. in physics from the College of William and Mary, Virginia, in 1985. He was a postdoctoral fellow (1985–1988) and is now a staff member of the Solid State Theory group at the Solar Energy Research Institute.

Alex Zunger received his Ph.D. in chemical physics from the Tel Aviv University, Israel, in 1975. He did postdoctoral work at Northwestern University (1975–1977) and the University of California, Berkeley (1977–1978). He joined the Solar Energy Research Institute in 1978, where he is a principal scientist and group leader of the Solid State Theory group.

SUBJECT AREA EDITOR

Thomas A. Kitchens

REFERENCES

Barker, J. A. 1953. *Proc. Roy. Soc. London* 216:45.

Bendt, P., and Zunger, A. 1982. *Phys. Rev. B* 26:3114.

Bragg, W. L., and Williams, E. J. 1934. *Proc. Roy. Soc. London Ser. A* 145:699.

Chadi, D. J., and Cohen, M. L. 1973. *Phys. Rev. B* 8:5747.

Connolly, J. W. D., and Williams, A. R. 1983. *Phys. Rev.* 27:5169.

Dandrea, R. G., Bernard, J. E., Wei, S.-H., and Zunger, A. 1990. *Phys. Rev. Lett.* 64:36.

Ferreira, L. G., Mbaye, A., and Zunger, A. 1987. *Phys. Rev. B* 35:6475.

Ferreira, L. G., Mbaye, A., and Zunger, A. 1988. *Phys. Rev. B* 37:10547.

Ferreira, L. G., Wei, S.-H., and Zunger, A. 1989. *Phys. Rev. B* 40:3197.

Finel, A., and Ducastelle, F. 1984. *Mat. Res. Soc. Symp. Proc.* 21:293.

Hohenberg, P., and Kohn, W. 1964. *Phys. Rev.* 136.

Ihm, J., Zunger, A., and Cohen, M. L. 1979. *J. Phys. C* 12:4409.

Ishida, K., Shumiya, T., Nomura, T., Ohtani, H., and Nishizawa, T. 1988. *J. Less Comm. Metals* 142:135.

Jen, H. R., Cherng, M. J., and Stringfellow, G. B. 1986. *Appl. Phys. Lett.* 48:1603.

Jen, H. R., Cherng, M. J., and Stringfellow, G. B. 1987. *J. Crystal Growth* 85:175.

Kanamori, J., and Kakehashi, Y. 1977. *J. Physique* 38(7):274.

Kikuchi, R. 1951. *Phys. Rev.* 81:988.

Kikuchi, R. 1974. *J. Chem. Phys.* 60:1071.

Kikuchi, R., Sanchez, J. M., de Fontaine, D., and Yamaguchi, H. 1980. *Acta. Metall.* 28:651.

Kuan, T. S., Kuech, T. F., Wang, W. I., and Wilkie, E. L. 1985. *Phys. Rev. Lett.* 54:201.

Martins, J. L., and Zunger, A. 1986. *J. Mat. Res.* 1:523.

Nakayama, H., and Fujita, H. 1986. In *Proc. 12th internat. symp. on GaAs and related compounds,* Inst. Phys. Conf. Ser. *79,* edited by M. Fujimoto. London: Institute of Physics, p. 289.

Panish, M. B., and Ilegems, M. 1972. *Prog. Solid State Chem.* 7:39.

Sanchez, J. M., Ducastelle, F., and Gratias, D. 1984. *Physica* 128A:334.

Srivastara, G. P., Martins, J. L., and Zunger, A. 1985. *Phys. Rev. B* 31:2561.

Stringfellow, G. B. 1973. *J. Phys. Chem. Solids* 37:1749.

Styre, D. F., Phani, M. K., and Lebowitz, J. 1986. *Phys. Rev. B* 34:3361.

Wei, S.-H., and Krakauer, H. 1985. *Phys. Rev. Lett.* 55:1200.

Wei, S.-H., Ferreira, L. G., and Zunger, A. 1990. *Phys. Rev. B* 41:8240.

Wood, D. M., and Zunger, A. 1985. *J. Phys. A* 18:1343.

Zunger, A. 1986. *Internat. J. Quant. Chem.* 19:629.

Zunger, A., and Wood, D. M. 1989. *J. Crystal Growth* 98:1.